geoconvention
Virtual Event
September 13 - 15
2021

Virtual Petrophysical Laboratory – Part 2: Testing and Simulation

Leon Fedenczuk[1], Kristina Hoffmann[1], and Tom Fedenczuk[2]

[1]Gambit Consulting Ltd., [2] Abakai International.

Abstract

This paper presents results of the advanced testing and simulation in a computer based petrophysical laboratory of porous media done directly in 3D space. The foundation of the system was presented in the first part of the paper (Leon Fedenczuk, at al 2020) during Geoconvention 2020. Tests start with estimates for the total porosity, effective porosity, tortuosity, which are followed by resistivity estimates and capillary pressure curves simulation. The saturations of the wetting and non-wetting fluids are recorded for each pressure. At each step of the drainage and imbibition process, nine values of electrical resistivity are estimated. In addition, tortuosity statistics are calculated during capillary pressure tests. The presented results and visualization show how correlated porosity and layered structures affect estimated properties, the capillary curve hysteresis, and 3D shapes of the non-wetting fluid paths at break-through events.

Capillary Pressure Curves and Resistivity

During fluid displacement testing, the system first checks whether the empty voxels form branches of the pore network, which connect (span) two opposite faces of the model. The modeling and simulations are performed using connectivity algorithms for the octree data structure (presented in Part 1).
Simulated capillary tests start with samples fully saturated with wetting fluid that is introduced only into the effective porosity, which corresponds to actual laboratory tests (Mohsen Masihi 2010). Next, wetting and non-wetting fluids interact under varying pressure. The 3D simulation process records the effective porosity that is occupied by the wetting and non-wetting phase at different pressure values. Special connectivity algorithms find dimensions of pore space and connectivity to corresponding fluid sources at each pressure in a series of mini-steps. This supports simulating trapping mechanisms where one of the fluids is surrounded by the other fluid type. At each pressure the interface locations are marked and their movement is controlled by the effective pore radius relative to the current pressure value.

At each pressure, nine values of electrical resistance are derived from the properties of the voxels at the lowest octree level through recursive upscaling algorithms by a depth-first tree traversal. This aggregates the properties of each eight nodes/voxels starting from the leaf level on the tree and progressively working toward the top of the tree. At every step, each voxel resistance is represented by resistors, which form a larger resistor network. This implemented upscaling process can stop if intermediate results at the courser grid are desirable. Figure 1 shows nine estimates of the formation factor for a layered sample presented in Part 1.

The resistivity estimates come from three different configurations of electrical circuits that represent each voxel. In the first two methods, each voxel is represented by a single resistor, whose resistance is a function of the medium resistance and voxel size. The interconnections between these voxels are approximated in the form of chain models or bundle models. These two models correspond to the earliest methods of the porous media simulations and upscaling with bundles of pipes, which are similar to geometrical and harmonic averaging.

In the third novel method designed for this project, voxels are replaced by sets of six resistors organized as 3D crosses. This corresponds to simulations of porous media with a regular cubic lattice, which corresponds to a network coordination number of six. The extended local network is built from a set of eight voxels which have the same parent and are replaced by 48 element circuit used in the estimation of the effective resistance in horizontal and vertical directions. The nodal analysis is applied to this circuit to solve for voltages at electrical nodes which correspond to connections between resistors of the network.

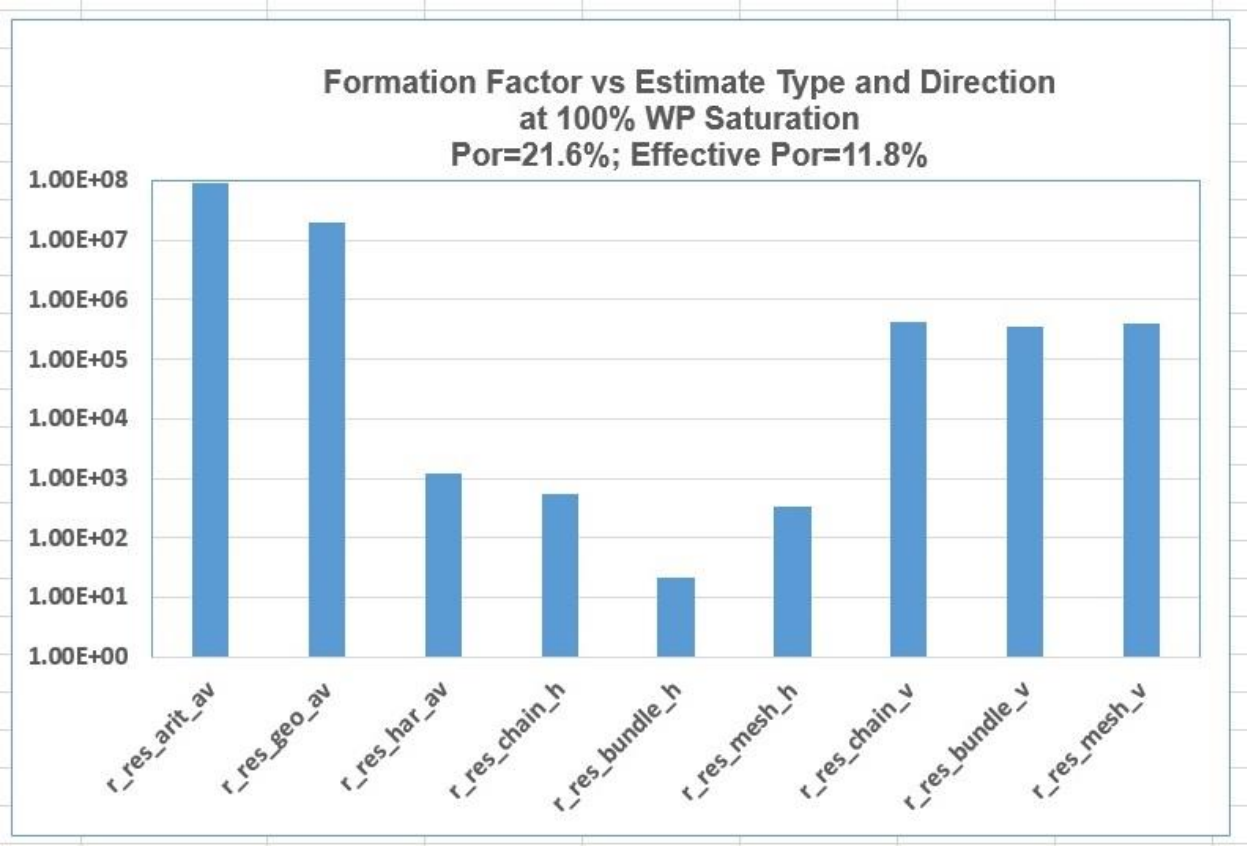

Figure 1. Nine Formation Factor estimates for the layered sample (‘B’). From left: arithmetic average, geometric average, harmonic average, horizontal chain/bundle/mesh, and vertical chain/bundle/mesh.

This resistivity estimate process accounts for 3D pore structure connectivity, fluid types, and local path sizes relatively to the pressure values. Solid matrix properties are included in computations based on their properties. Figure 1 shows drastic differences between upscaling estimates for the layered model (sample 'B' – layered sample with correlated pore space). Arithmetic and geometric averages are too high, while the harmonic average seems more reasonable. Estimates based on our new algorithms (chain, bundle, and mesh) show large differences between horizontal and vertical estimates in the next two groups of reported values. The values of the mesh algorithm fall between values from the chain and bundle horizontal estimates. The mesh horizontal estimates are similar to harmonic averages.

In comparison, the statistical harmonic averages are equal in both directions (horizontal and vertical), while our algorithms account for heterogeneity and estimate separate values for each flow direction.

The next graph (Figure 2) shows wetting-phase saturation pressure curves during drainage and imbibition for the correlated ('A') and correlated-layered ('B') samples, which simulate primary drainage and spontaneous imbibition processes. During the drainage process, saturation level corresponds to capillary pressure associated with smaller pores. Larger pores are affecting capillary pressure during the imbibition process.
Above results indicate the following:

- Sample 'A' shows lower threshold pressure (which is the lowest pressure at which the non-wetting phase starts displacing the wetting phase) and higher irreducible water saturation compared to sample 'B'.
- Sample 'A' is also characterized by a longer transition zone (which is the zone of changing water saturation with the height above the free water level).
- The size of the transition zone depends on rock characteristics like pore size distribution, grain sorting, porosity and permeability.
- During the imbibition process, part of non-wetting phase (oil) remains trapped in pore space as discontinuous (trapped) blobs. Remaining residual oil (Sor) is higher in sample 'B' (22%) comparing with sample 'A' (18%).

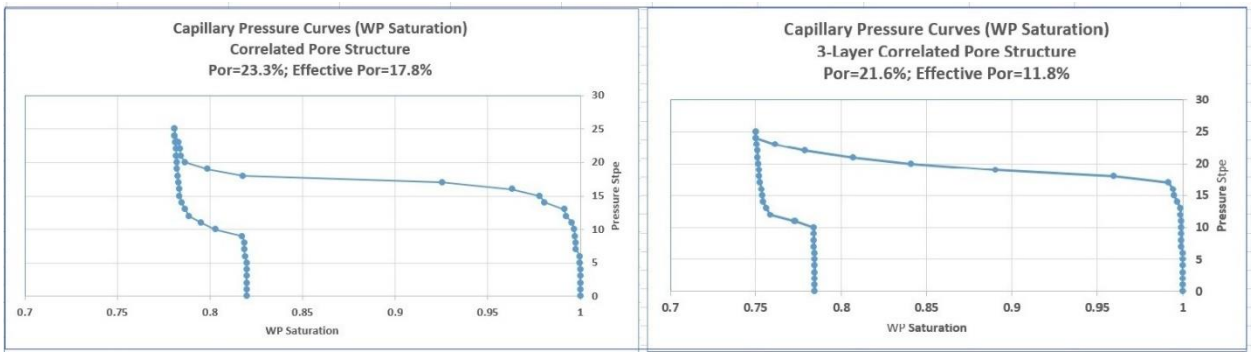

Figure 2 Wetting phase saturation recorded during drainage and imbibition in sample 'A' and 'B'.

The electrical resistivity simulation for the correlated 'A' sample in horizontal and vertical directions were different but not as drastically different when comparing these estimates for the layered sample (see Figure 3). This effect can be only detected using our novel mesh method. The graph in Figure 3 shows that estimates of the vertical electrical resistivity in sample 'B' were very high at all pressure values. On the other hand, the horizontal resistivity showed hysteresis similar to the case with the wetting phase saturation when simulating the drainage and imbibition parts.

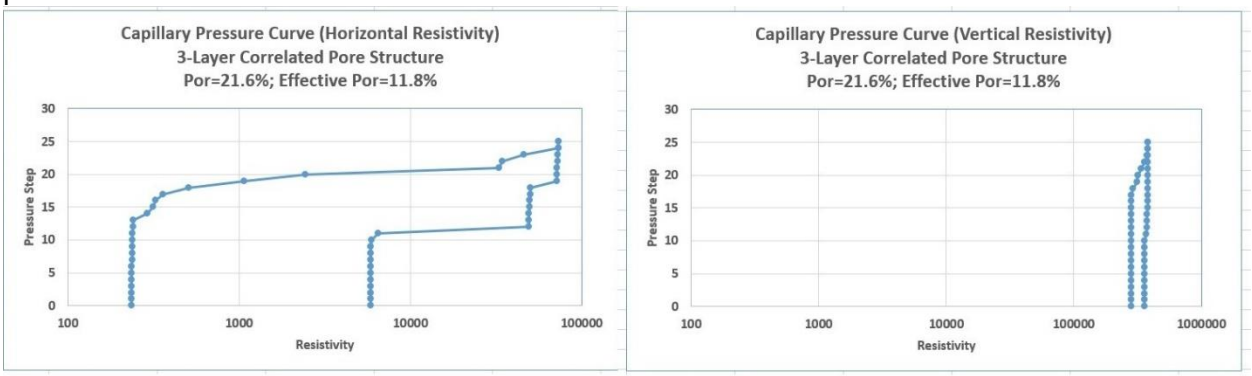

Figure 3. Horizontal and vertical resistivity recorded during drainage and imbibition in sample 'B' using the mesh method.

Tortuosity

Figure 4 shows the path-length statistics for the layered sample. The graph shows a group comparison between the average, minimum, and maximum statistics for the drainage process marked as L, while R represents estimates for the imbibition process. These processes start from the left face and right face respectively.

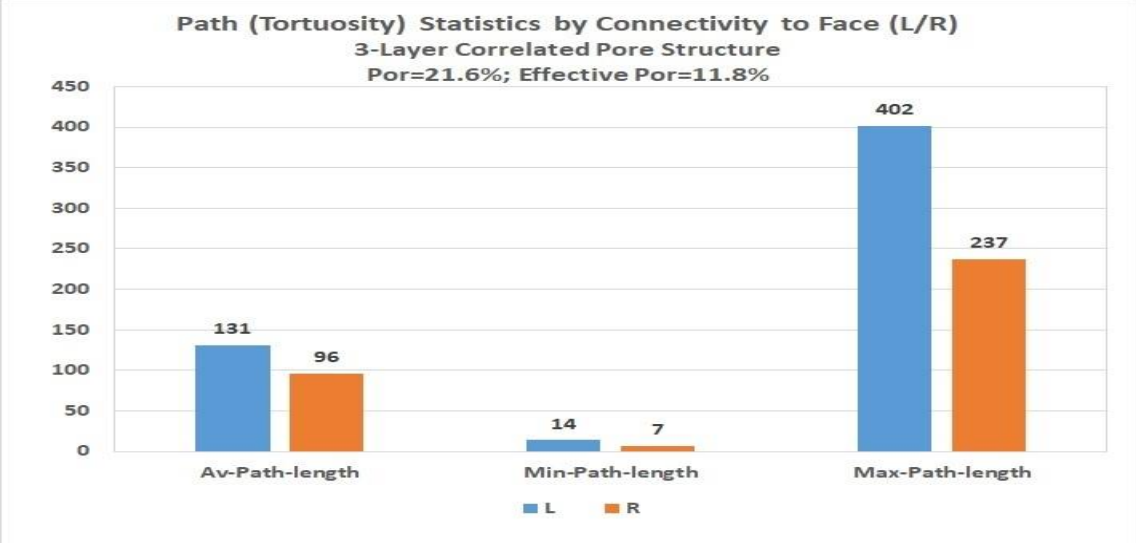

Figure 4. Path length (tortuosity) statistics of the correlated and layered model during drainage (L) and imbibition (R) processes.

Prior to the simulation, the active/effective network was detected and marked. Next, the path statistics are estimated in both drainage and imbibition tests. The path count and length are recorded for each individual process that starts at one of the faces of the model and ends on the opposite face. The path count advances only when the voxels on the opposite faces have not yet been filled-in by the invading fluid.
The imbibition path statistics are systematically smaller due to the wetting phase following already established continuous non-wetting network by shortest paths possible. These estimates are done directly in the 3D space while actual laboratory estimates are done by non-direct methods.

Summary

This paper shows that the same volume data structure (octree) could be used to model, simulate, and visualize porous models and their physical properties. The connectivity algorithms in octrees form a basis for the simulation of fluid interaction during drainage and imbibition. In addition, they are used in upscaling/estimating sample properties. They are applied to find an interconnected path between two faces of a sample and calculate the effective radius that is used to test for the interface movements. Our system estimates saturations and compares nine values of resistivity for a sample, based on properties of both fluids in the pore space and rock matrix, as a function of the pressure. The differences between these estimates indicate uncertainties, which can lead to better selection of boundaries in the up-scaled properties that are passed to reservoir simulations.

Different model structures result in varying degrees of the hysteresis in the saturations of both fluids and electric properties that change with pressure during the drainage-imbibition cycle. Our novel mesh algorithm for estimating electrical properties performed the best when estimating differences between horizontal and vertical measurements for layered structures. Enhanced visualization of geometrical properties improves the interpretation of simulation results. Visualization showed that the simulation process resulted in the partial retraction from pores and trapping of two phases. The results obtained here are consistent with observations in real porous media experiments and results published in a variety of papers.

Furthermore, all simulations and estimates can be run using different assumptions and process schemas while working with exactly the same model. In summary, the concept and algorithms developed here open new research opportunities in finding a variety of relationships between the structure of porous media and the resulting physical properties. Finally, permeability evaluations can be made by substituting permeability for the electrical conductivity or by using known relationships between the permeability and conductivity for specific rock types.

References

Leon Fedenczuk and Kristina Hoffmann, GeoConvention 2020, paper 55771, Virtual Petrophysical Laboratory – Part1: Modeling and Visualization.

Mohsen Masihi 2010, Laboratory Work Book No. 26504, Sharif University of Technology, Tehran, Iran.